

Conformational properties of chiral tobacco alkaloids by DFT calculations and vibrational circular dichroism: (−)-S-anabasine

P.G. Rodríguez Ortega, M. Montejo *, F. Márquez, J.J. López González

Physical and Analytical Chemistry Department, Experimental Science Faculty, University of Jaén, Campus “Las Lagunillas”, Ed. B3, Jaén E-23071, Spain



ARTICLE INFO

Article history:

Received 28 January 2015

Received in revised form 15 May 2015

Accepted 22 May 2015

Available online 27 May 2015

Keywords:

(−)-S-anabasine

Conformational profile

VCD

DFT

NBO

ABSTRACT

A thorough DFT and MM study of the conformational landscape, molecular and electronic structures of (−)-S-anabasine is reported aimed to reveal the mechanism controlling its conformational preference. Although the conformational flexibility and diversity of this system is quite extensive, only two structures are populated both in gas-phase and solution (CCl₄ and DMSO). NBO-aided electronic structure analyses performed for the eight conformers representing minima in the potential energy surface of (−)-S-anabasine indicate that both steric and electrostatic factors are determinant in the conformational distribution of the sample in gas phase. Nonetheless, hyperconjugative effects are the key force tipping the balance in the conformational equilibrium between the two main rotamers. Increasing the polarity of the medium (using the IEF-PCM formalism) barely affect the conformational energy profile, although a slight increase in the theoretical population of those structures more affected by electrostatic interactions is predicted. The validity of the theoretical models and calculated conformers populations are endorsed by the accurate reproduction of the IR and VCD spectra (recorded in pure liquid and in CCl₄ solution) of the sample (that have been firstly recorded and assigned in the present work) which are consistent with the occurrence of a 2:1 conformational ratio.

© 2015 Elsevier Inc. All rights reserved.

1. Introduction

Nicotinoids (*i.e.* alkaloids having in common a two-ring assembly with a 3-pyridyl methylamine skeleton) constitute a group of biochemically relevant compounds that have been found to be bioactive as agonists of the acetylcholine receptor (nAChR). Some compounds of this group have even demonstrated their applicability in the treatment of numerous diseases such as Alzheimer, schizophrenia, Parkinson, Tourette's syndrome, anxiety, cognitive and attention deficits, and smoke addiction [1–9].

It has been established that the agonist-nAChR interaction is mediated by either hydrogen bonding or cation-π contact [9–11] and depends on the agonist's intramolecular N...N distance, which is conditional on the adopted molecular conformation. This fact convert the molecular and electronic structure of alkaloids in important issues of study: a deep knowledge of the structural properties of these compounds may not only help getting a better insight into the mechanism of the molecular recognition processes in which they are involved, but also would be relevant for the

subsequent design of structurally related systems with potential biomedical interest.

These reasons explain the number of studies in scientific literature dealing with the molecular structure and conformational preferences in nicotinoids, [12–29] albeit a vast majority of the work in this field has been devoted to nicotine.

(−)-S-anabasine (one of the minority piperidinic nicotinoids in tobacco leaves, ~0.5%) has also been reported to have interesting biomedical applications [30] and its molecular structure and spectroscopic properties have been the target of several works [31–36].

Despite these previous efforts, some interesting issues such as the nature of the stereoelectronic effects controlling the conformational equilibrium in the system and how it may result affected by the polarity of the surrounding medium remain still unexplored.

In order to overcome this lack of information, we report a thorough structural and conformational analysis of (−)-S-anabasine both under the isolated molecule approximation and in solution (using the IEF-PCM formalism) considering non-polar and polar solvents (*i.e.* CCl₄ and DMSO), that also comprises the implementation of the Natural Bond Orbitals (NBO) methodology for the analysis of the electronic structure of the different molecular conformations of the species.

The experimental validation of our theoretical models has been obtained from the analysis of the first records of the Vibrational

* Corresponding author.

E-mail address: mmontejo@ujaen.es (M. Montejo).

Circular Dichroism (VCD) spectra of the species, both in pure phase and in solution, which have been recorded and thoroughly analyzed. This technique represents one of the most sensitive forms of vibrational spectroscopy and has recently proven to be a more powerful conformer-discriminating tool than its non-chirality sensitive counterpart, FTIR, when studying the solution-state conformer distribution of other structurally related nicotinoids. [37,38]

2. Methods and materials

2.1. Theoretical methods

The MMFF [39–43] and SYBYL [44] force fields as implemented in SPARTAN08 program package [45] were used to carry out the conformational search employing the Monte-Carlo methodology. A total of 22 structures were generated and those non-redundant structures of lower energy were selected for a further geometrical optimization (with *ab initio* and DFT quantum chemical calculations) and the computation of their harmonic vibrational frequencies using Gaussian09 (Revision D. 01) [46]. SCF=tight and Int=Ultrafine were the convergence criteria chosen during the geometry optimization. The Becke's three-parametric hybrid exchange functional [47] combined with the Lee–Yang–Parr correlation functional [48] and with the exchange component of Perdew and Wang' 1991 functional [49–51] (i.e. B3LYP and B3PW91 hybrid functionals) were used in conjunction with the 6-311++G** [52] and aug-cc-pVTZ [53] basis sets. MP2 method [54] in conjunction with 6-31+G* basis set [55,56] was implemented in order to validate minima. Natural Bond Orbital (NBO) [57] calculations were accomplished using the program NBO v.6.0. [58]. Solvent modeling were performed applying the integral equation formalism of the polarizable continuum solvation model (IEF-PCM method [59–63]), using the dielectric constants corresponding to CCl₄ ($\epsilon = 2.2$) and dimethylsulfoxide ($\epsilon = 46.8$), and with a cavity build up using UFF radii (explicit treatment for hydrogen atoms) as implemented in Gaussian 09. All simulated spectra were broadened according to a Lorentzian function with a full width at half maximum (FWHM) of 8 cm⁻¹.

2.2. Experimental procedure

Samples of (–)-S-anabasine (94%) (pale orange liquid at room temperature) were purchased from Alfa-Aesar and used without further purification

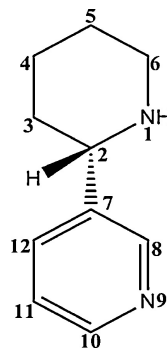


Fig. 1. Molecular structure and atom numbering of (–)-S-anabasine molecule.

The mid-IR and VCD spectra (neat liquid and CCl₄ solution) were recorded using a JASCO FVS-4000 VCD spectrometer and demountable standard liquid cells equipped with BaF₂ windows, using a spectral resolution of 4 cm⁻¹ and 4000 scans. The device is equipped with a MCT detector for measurements in the 2000–900 cm⁻¹ range and an InSb detector for the 4000–2600 cm⁻¹ range. The concentration of the CCl₄ solutions (1–2M) and path-lengths (5–50 μm) were optimized as recommended elsewhere [64,65] to get the optimum absorbance for the VCD and IR measurements (kept in the range 0.12–0.9). Baseline corrections were accomplished by subtracting the pure solvent raw spectrum recorded under the same experimental conditions. The IR/VCD spectra of the pure liquid were recorded using a 6 μm path-length. In this case, the spectra recorded for the empty cell was used for baseline corrections.

3. Results and discussion

3.1. Molecular conformations and gas-phase conformer distribution.

The search for minima in the potential energy surface of (–)-S-anabasine (see Fig. 1 for atom numbering) was carried out by means of a direct strategy consisting on exploring all the possible sources of conformational diversity: the piperidine ring conformation, the axial or equatorial arrangement of the N1–H and C2–Pyr bonds and the relative internal rotation of the pyridine ring (that may adopt the so-called A and B orientations). Fig. 2 displays a scheme

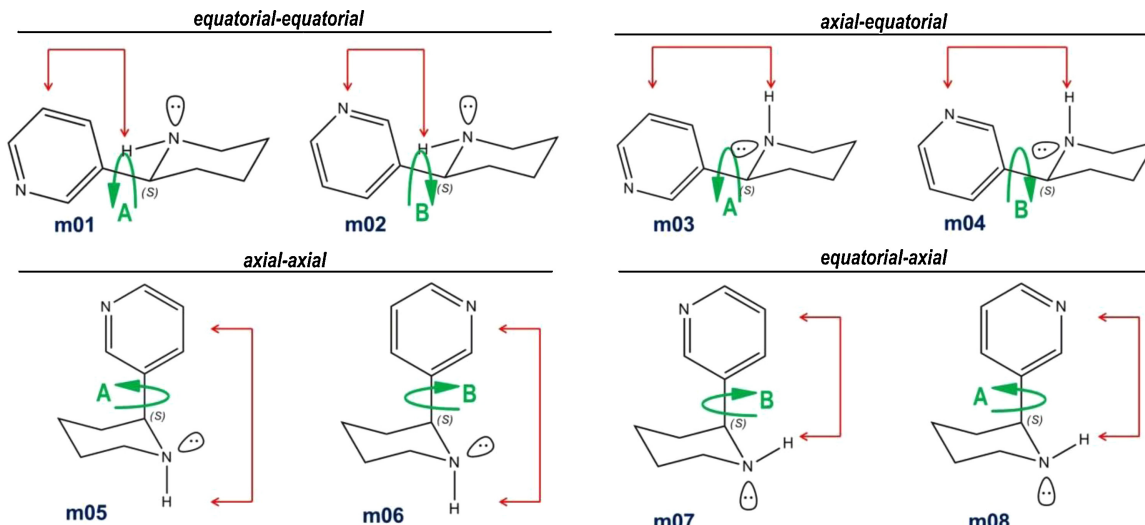


Fig. 2. Schematic representation of conformers taken into account in direct DFT conformational search of (–)-S-anabasine.

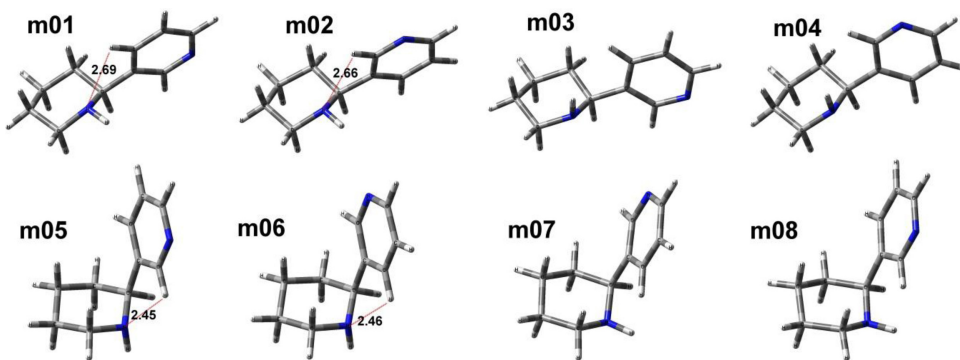


Fig. 3. Optimized structures of conformers for (*-*)-S-anabasine molecule at the B3PW91/aug-cc-pVTZ level of theory.

that relates the commented molecular flexibility sources with the subsequent set of potential conformers considered.

Hence, our initial guess consisted of eight different structures which were optimized at the B3LYP/6-31+G* level of theory. The absence of imaginary frequencies in their computed harmonic vibrational spectra confirmed them as real minima on the potential energy surface. In all of them the piperidine ring adopts two different (see below) chair-like conformation.

The consistency of these results was confirmed by a Monte-Carlo based molecular mechanics search (MMFF and SYBYL force fields). From the 22 structures found, the optimization of the non-redundant generated structures with lower calculated energies (within 7 kJ mol⁻¹) led us to the same set of conformers already characterized as minima by DFT calculations, allowing us to discard, for example, structures with twisted-boat conformation of the piperidine ring (lying 23–33 kJ mol⁻¹ higher in energy). Their molecular structures, depicted in Fig. 3, reproduce those previously proposed for (*-*)-S-anabasine in Ref. [35] Cartesian coordinates of the eight conformers (B3PW91/aug-cc-pVTZ, gas phase) are available as supplementary material (Table S3).

According to the values of their main geometrical parameters, these eight conformers can be organized in pairs. Thus, the conformers denoted as m01/m02 are characterized by the equatorial orientation of both the N1-H and C2-Pyr bonds leading to eq-eq structures only differing in the rotation of the pyridine ring. Similarly, the molecular structures of the other three pairs of conformers, namely, m03/m04 (ax-eq), m05/m06 (ax-ax) and m07/m08 (eq-ax) also differ mainly in the pyridine ring internal rotation, that can be characterized for the C2-C7-C8-N9 dihedral angle which adopts values of opposite sign between each pair of conformers.

The two possible chair-like structures of (*-*)-S-anabasine conformers are defined by the position adopted by the N1 atom respect to the plane formed by the atoms C2, C3, C5, and C6 that is: *ca.* 28° above the plane for conformers m01 to m04, and *ca.* 25° below the plane for conformers m05–m08.

Relative Gibbs free energies (ΔG , kcal mol⁻¹) and corresponding Boltzmann's populations calculated in gas-phase for the set of conformers are collected in Table 1. DFT calculations indicate that conformers m01 and m02 (eq-eq) are the most stable structures in gas-phase, being the energy difference between them of 2.05 kJ mol⁻¹ (B3PW91/aug-cc-pVTZ). The pairs m03/m04, m05/m06 and m07/m08 are *ca.* 10.45, 18.81 and 22.99 kJ mol⁻¹ above the global minimum, respectively.

Results obtained regarding relative energies and populations with the four methods used are comparable and all of them calculate a substantially higher abundance for m01 and m02 structures that account up to the 98.02% of the total sample composition (68.09% m01 + 29.93% m02, B3PW91/aug-cc-pVTZ). The residual 2% of the total gas-phase composition correspond to the rela-

Table 1

Relative energies (ΔG in kJ mol⁻¹) and Boltzmann's populations (%) calculated in gas-phase, CCl₄ and DMSO solutions (IEF-PCM) using B3LYP and B3PW91 at 298.15 K for (*-*)-S-anabasine set of conformers.^{a,b}

	B3LYP/aug-cc-pVTZ		B3PW91/aug-cc-pVTZ	
	ΔG Gas-phase	%Pop.	ΔG	%Pop.
m01	0.00	67.53	0.00	68.09
m02	2.04	29.75	2.04	29.93
m03	10.45	1.00	10.41	1.02
m04	9.20	1.65	10.74	0.89
m05	19.81	0.02	19.73	0.02
m06	19.27	0.03	18.48	0.04
m07	22.95	0.01	22.28	0.01
m08	23.03	0.01	22.36	0.01
CCl ₄				
m01	0.00	66.11	0.00	66.06
m02	1.92	30.55	1.88	31.04
m03	8.69	1.99	9.15	1.64
m04	9.82	1.26	10.07	1.14
m05	21.15	0.01	18.64	0.04
m06	17.35	0.06	17.30	0.06
m07	22.61	0.01	21.90	0.01
m08	22.57	0.01	21.94	0.01
DMSO				
m01	0.00	52.37	0.00	52.05
m02	0.63	40.83	0.63	40.54
m03	6.06	4.56	6.06	4.52
m04	7.86	2.19	7.23	2.81
m05	20.02	0.02	19.06	0.02
m06	19.39	0.02	18.43	0.03
m07	21.57	0.01	20.90	0.01
m08	21.74	0.01	21.15	0.01

^a Theoretical population calculated using the Boltzmann's equation and taking T=298.15 K.

^b Absolute values of E_0 energies (gas phase) are collected in Table S2 in Supplementary information.

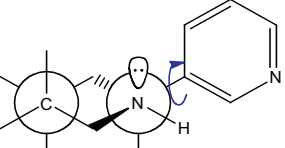
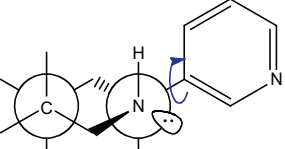
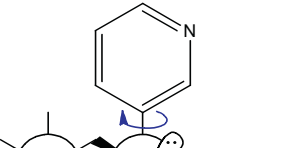
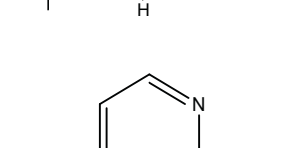
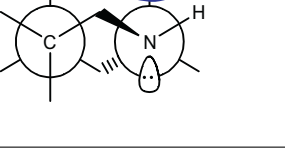
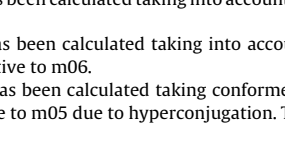
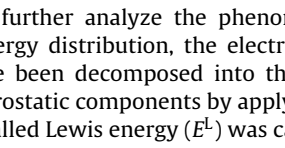
tive population calculated for m03 and m04 conformers (1.02% m03 + 0.89% m04, B3PW91/aug-cc-pVTZ). The remaining structures are much higher in energy, being not energetically reachable at room temperature. This theoretical gas-phase sample composition is comparable with those previously reported. [35]

3.2. Electronic structures and conformational preference

A global view of both molecular geometries and relative Gibbs free energies allows to tentatively set a geometrical priority trend for the preferred conformations in (*-*)-S-anabasine (see Table 2). As shown, the most stability-determining geometrical factors seem to be related to the arrangement of the C2-Pyr bond and the conformation adopted by the saturated heterocycle. Indeed, the equatorial orientation of this group is a common feature in the

Table 2

Schematic representation of the relative arrangement of N-H and pyridine groups in the set of conformers of (−)-S-anabasine related to their calculated relative stability. Geometrical priority trend for the preferred conformations in (−)-S-anabasine and relative NBO Lewis, non-Lewis Steric and electrostatic energies (in kJ mol^{-1}) calculated for the set of conformers of (−)-S-anabasine taking the optimized structures at the MP2/6–31+G* level.

Conformer		ΔE_e^{SCF}	NBO analysis				
			$\Delta E^{\text{L}\text{a}}$	$\Delta E^{\text{S}\text{b}}$	$\Delta E^{\text{E}\text{c}}$	$\Delta E^{\text{NL}\text{d}}$	
m01		eq-eq	0.00	8.44	10.91	16.38	-19.02
m02			2.59	0.00	12.87	5.98	-7.98
m03		ax-eq	14.29	28.26	0.00	47.11	-24.58
m04			11.12	10.45	10.28	19.02	-9.91
m05		ax-ax	24.08	13.50	32.27	0.08	0.00
m06			21.94	17.39	36.24	0.00	-6.02
m07		eq-ax	27.67	32.39	31.39	19.85	-15.26
m08			27.46	31.14	30.93	19.06	-14.25

^a Relative ΔE^{L} has been calculated taking into account the Lewis energy of conformer m02 (which has the lower Lewis energy) as reference; hence $\Delta E^{\text{L}} > 0$ stand for destabilization relative to m02.

^b Relative ΔE^{S} has been calculated taking into account conformer m03 as reference since it is the structure with lower steric repulsions; hence $\Delta E^{\text{S}} > 0$ means destabilization relative to m03.

^c Relative ΔE^{E} has been calculated taking into account conformer m06 as reference since it is the structure with lower electrostatic repulsions, hence $\Delta E^{\text{E}} > 0$ means destabilization relative to m06.

^d Relative ΔE^{NL} has been calculated taking conformer m05 (which is the structure less stabilized by hyperconjugative interactions) as reference; hence $\Delta E^{\text{NL}} < 0$ means stabilization relative to m05 due to hyperconjugation. The negative value of ΔE^{NL} stands for its stabilizing nature.

four conformers of lower energy which, besides, have the same chair-like ring structure.

In order to further analyze the phenomena governing conformational energy distribution, the electronic energies of each conformer have been decomposed into their Lewis, non-Lewis, steric and electrostatic components by applying the NBO methodology. The so-called Lewis energy (E^{L}) was calculated removing all Rydberg and antibonding orbitals from the NBO basis set so that the energies corresponding to the ideal Lewis structures of the systems were obtained. Steric contributions to the Lewis energies (E^{S}) were calculated by using the STERIC utility implemented in NBO 6.0 package [58], being the electrostatic repulsions (E^{E}) determined according to: $E^{\text{L}} = E^{\text{S}} + E^{\text{E}}$. Stabilizing non-Lewis energies (E^{NL}) were calculated accounting for all the possible donor–acceptor interactions in each structure.

Data reported in Table 2 show the dominant effect that steric interactions have in the conformational preference in this species. Nonetheless, the relative stability of eq-eq structures (m01 and m02), which are characterized by lower Lewis energies than the remaining conformers, is controlled by delocalization effects: Lewis energy favors m02 by 8.44 kJ mol^{-1} (MP2/6–31+G*) while non-Lewis delocalizations stabilize conformer m01 over m02 by $11.03 \text{ kJ mol}^{-1}$ (MP2/6–31+G*) indicating that the balance of the conformational equilibrium between this two species is tipped by hyperconjugative effects (the global electronic energy difference calculated for them is 2.59 kJ mol^{-1} at the MP2/6–31+G* level).

In the remaining conformers, the contribution of hyperconjugative delocalizations, in some cases larger than for conformers m01/m02, does not compensate their higher Lewis energies. For instance, conformer m03 is the structure with lower steric repul-

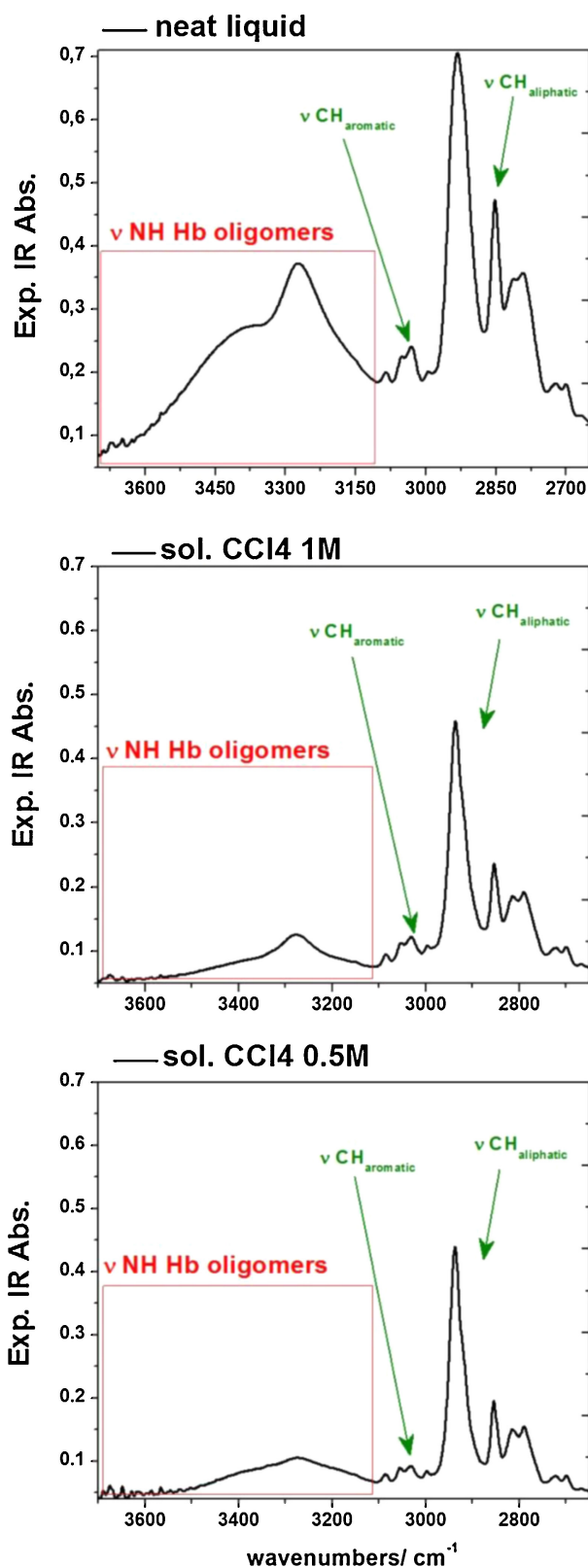


Fig. 4. Experimental IR spectra recorded for the pure liquid (*-*)-S-anabasine and CCl_4 solutions with concentrations ranging from 1 M to 0.5 M. Path lengths of 6 μm have been used for the neat liquid sample and 12 μm for the sample solutions.

Table 3

Experimental bands observed for (*-*)-S-anabasine (in the pure liquid spectra) along with their theoretical correspondence (calculated in gas-phase at the B3PW91/aug-cc-pVTZ level) and their proposed assignment.

Exp. $\nu \text{ cm}^{-1}$	Scaled Theo. $\nu \text{ cm}^{-1}$		NVM ^b
	B3PW91/ aug-TZ gas ^a	m01	
1592	1585	1586	$\delta^{\text{ip}}\text{CH}^{\text{PYR}} + \nu\text{CC}^{\text{PYR}}$
1578	1567	1567	$\delta^{\text{ip}}\text{CH}^{\text{PYR}} + \nu\text{CC}^{\text{PYR}}$
1478	1460	1459	$\delta^{\text{ip}}\text{CH}^{\text{PYR}} + \nu\text{CC}^{\text{PYR}}$
	1445	1445	scCH_2
1469	1433 1432	1433 1431	$\delta\text{NH} + \text{scCH}_2$
1442	1423	1423	scCH_2
1425	1413 1410	1415 1410	$\text{scCH}_2 + \delta^{\text{ip}}\text{CH}^{\text{PYR}}$
1372	1350	1349	waCH_2
1354	1336	1335	$\delta^{\text{ip}}\text{CH}^{\text{PYR}} + \text{waCH}_2$
	1328	1328	waCH_2
	1315	1314	waCH_2
1329sh	1307	1307	$\text{waCH}_2 + \delta^{\text{ip}}\text{CH}^{\text{PYR}}$
1319	1299	1304	$\delta^{\text{ip}}\text{CH}^{\text{PYR}}$
1300	1281	1281	$\delta^{\text{C*H}} + \text{twCH}_2$
1267	1263	1258	$\nu\text{CC}^{\text{PYR}} + \text{twCH}_2$
1257	1245	1245	twCH_2
	1227	1225	$\delta^{\text{ip}}\text{CH}^{\text{PYR}} + \text{twCH}_2 + \text{breath}^{\text{PYR}}$
1218sh	1200	1191	$\delta^{\text{C*H}} + \delta^{\text{ip}}\text{CH}^{\text{PYR}}$
1211	1187	1187	twCH_2
1184	1173	1178	$\delta^{\text{ip}}\text{CH}^{\text{PYR}}$
1150	1128	1128	twCH_2
1116sh	1109	1111	$\delta^{\text{ip}}\text{CH}^{\text{PYR}} + \text{twCH}_2$
1106	1097	1101	$\delta^{\text{ip}}\text{CH}^{\text{PYR}} + \text{twCH}_2$
1064	1085	1085	ρCH_2
1050	1043	1043	$\delta^{\text{C*H}} + \rho\text{CH}_2$
1024	1033 1032	1034 1032	$\nu\text{CC}^{\text{pip}}$
	1006	1006	$\nu\text{CC}^{\text{PYR}} + \rho\text{CH}_2$
998	999	998	$\rho\text{CH}_2 + \nu\text{CC}^{\text{pip}} + \nu\text{CC}^{\text{PYR}}$
	981	977	$\delta^{\text{oop}}\text{CH}^{\text{PYR}}$
	951	950	$\delta^{\text{oop}}\text{CH}^{\text{PYR}}$
932	924	928	$\delta^{\text{oop}}\text{CH}^{\text{PYR}}$
917	910	910	ρCH_2
	902	902	$\delta^{\text{oop}}\text{CH}^{\text{PYR}}$

^a Scaled theoretical wavenumbers calculated for conformers of (*-*)-S-anabasine in gas-phase at the B3PW91/aug-cc-pVTZ level (scale factor = 0.965 taken from the Computational Chemistry Comparison and Benchmark Database, CCCBDB). All modes have A symmetry.

^b Symbols used: ν = stretching, δ = deformation, ρ = rocking, sc = scissoring, tw = twisting, wa = wagging, breath = breathing, br = broad, sh = shoulder. Superscript * denote asymmetric carbon. Superscripts s and as denote symmetric and asymmetric motions of the NVM. Underscripts ip and oop denote in-plane and out-of-plane vibrational motions. Superscript PYR stands for pyridine ring. Superscript pip stands for piperidine ring. The description of the vibrational modes is proposed by means of their visual inspection using Gaussview 5.0.

sions, but the larger electrostatic interactions in this system make it barely abundant. Similarly, m05 and m06 are favored by the low magnitude of electrostatic interactions but the larger associated steric energies lead to their destabilization.

On the other hand, although the preference of a piperidine ring to adopt chair conformation with an equatorial orientation of the N1–H bond (as is the case of m01/m02) has been previously observed and explained on the basis of steric effects (*i.e.* lower Lewis

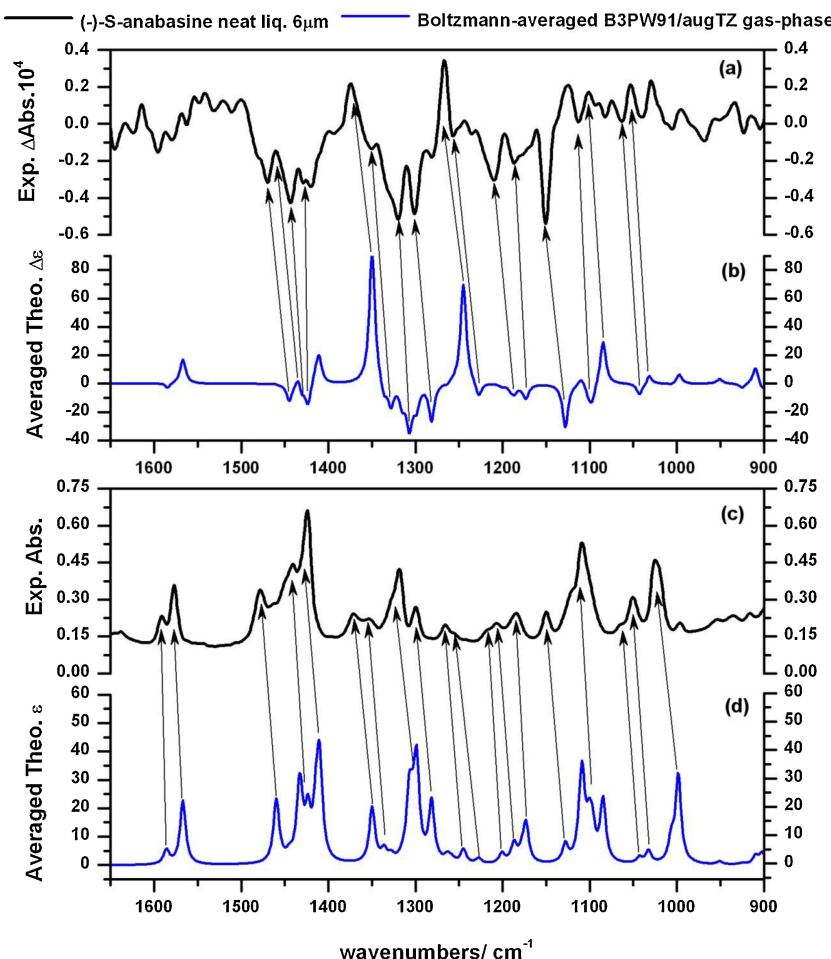


Fig. 6. Experimentally recorded VCD (a) and IR (c) spectra for pure (–)-S-anabasine (black lines) compared with the predicted VCD (b) and IR (d) scaled B3PW91/aug-cc-pVTZ Boltzmann-averaged spectra (blue lines) in the 1650–900 cm^{−1} region for a ca. 2:1 (m01:m02) conformational mixture of the sample in gas-phase. Boltzmann's populations at 298.15 K, Lorentzian fitted FWHM = 8 cm^{−1}, scale factor = 0.965 taken from the Computational Chemistry Comparison and Benchmark Database, CCCBDB. (For interpretation of the references to color in this figure legend, the reader is referred to the web version of this article.)

energies respect to ax structures) [66], it is noteworthy that the pair m07/m08 lies higher in energy than the pair m05/m06.

This unexpected higher stability of the ax-ax structures m05/m06 over the eq-ax conformers m07/m08 (despite presenting larger steric repulsions) could be related to the incidence of an intramolecular hydrogen bond (HBi) between the lone pair of the nitrogen atom in the piperidine ring and the closest H atom in the pyridine ring. In fact, the N...H calculated distances in m05 and m06 are 2.45 Å and 2.46 Å (B3PW91/aug-cc-pVTZ) respectively, values that are certainly within the range for such a weak interaction [67]. Besides, NBO detects electronic delocalizations from the lone pairs in N1 atom to the closest σ^* antibonding C–H orbital in pyridine ring in m05 and m06 with associated charge transfer orbital interaction energies ($E_{LP\sigma^*}^{(2)}$) of 4.51 and 4.30 kJ mol^{−1}, respectively.

At this point, it is worth to mention that authors in Ref. [35] also suggested that an N...H HBi may be responsible for the observed deviation from the ideal pyridine ring orientation in the two main conformers, namely m01 and m02. Other authors have also pointed to the occurrence of this type of interaction in related systems such as nicotine (Ref. [37] and references therein), protonated nornicotine (Ref. [68]) and methyl substituted nicotinoid derivatives (Ref. [69]). In our case, although the calculated N...H distances may also suggest the incidence of such interaction (2.69 Å and 2.66 Å, B3PW91/aug-cc-pVTZ) our analysis cannot confirm this assumption, since NBO did not plot any $N(LP) \rightarrow \sigma_{CH}^*$ stabilizing electronic

delocalization in m01 conformer, but a slight delocalization (2.21 kJ mol^{−1}) is predicted for conformer m02 (which has a shorter calculated N...H distance). This fact further endorses the idea that hyperconjugative effects are the main factor regulating the conformational preference toward the m01 form.

3.3. Effect of the surrounding medium in the molecular structure and conformational distribution

Calculations in solution (CCl₄, ϵ = 2.2; DMSO, ϵ = 46.8) indicate that the polarity of the solvent do not alter in large extent neither the molecular geometries of the conformers nor the conformational energy profile of (–)-S-anabasine. Fig. S1 (available as electronic supplementary information) shows how subtle are the geometrical differences between the structures of the four main conformers when going from gas-phase to DMSO solution.

Data reported in Table 1 show that, as in gas-phase, eq-eq structures (i.e. m01 and m02) are by far the most abundant species and would account for the 97.1% (66.06% m01 + 31.04% m02, B3PW91/aug-cc-pVTZ) of the total sample composition in carbon tetrachloride solution (remaining 3% is due to conformers m03 and m04). The larger polarity of DMSO produces a slight decrease in the relative population of m01 and m02 (92.6% B3PW91/aug-cc-pVTZ) and an increase in the relative abundances of m03 and m04 by more than a factor of 2, so their combined contribution to the

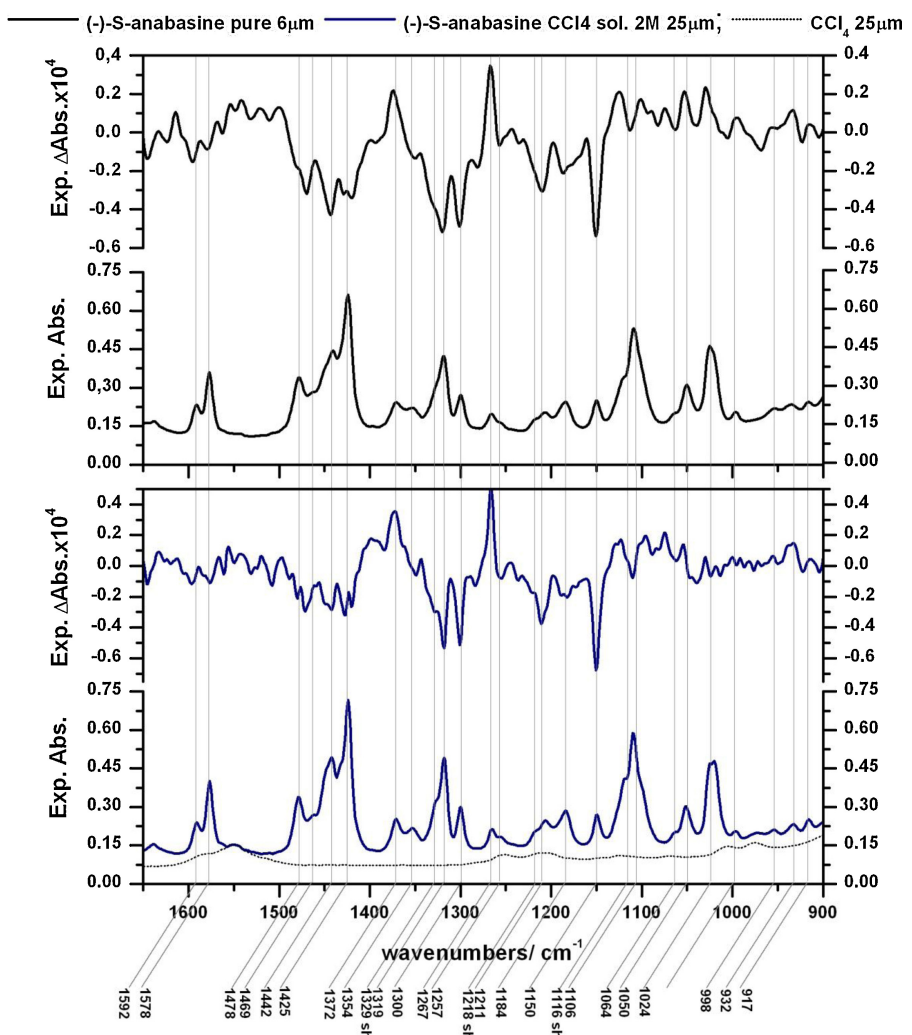


Fig. 5. Experimental VCD and IR spectra recorded for pure (–)-S-anabasine (top/black lines) and for its solutions in CCl_4 (bottom/blue lines). Wavenumbers of the corresponding experimental bands in each spectrum are marked and depicted below. Dash line corresponds to the spectrum recorded for the pure solvent. (For interpretation of the references to color in this figure legend, the reader is referred to the web version of this article.)

total sample composition would be 6.7% (B3PW91/aug-cc-pVTZ) in this solvent.

Calculated solvation energies (18.0 kJ mol^{-1} m01, 19.2 kJ mol^{-1} m02, 22.1 kJ mol^{-1} m03, 23.4 kJ mol^{-1} m04, B3PW91/aug-cc-pVTZ) indicate that ax-eq conformers (m03 and m04) are more stabilized than eq-eq structures (m01 and m02), possibly due to the minimization of Lewis-type interactions on going- from the gas-phase to DMSO solution. In fact, the stabilization of m03 and m04 species in DMSO relay on the fact that, according to NBO (see Table 2) relative stabilities and abundances of these conformers are controlled mainly by electrostatic effects (especially for m03 which is the more favored by increasing medium polarity). In any case, although DMSO is a highly polar solvent that would allow a strong minimization of electrostatic repulsions in m03 and m04, their contribution to the overall sample composition is still negligible even in this solvent.

3.4. Vibrational spectra of (–)-S-anabasine

Intended to assess the conformational composition of the sample, both in pure phase and in solution, the study of the IR and VCD spectra below is mainly focused in the $1650\text{--}900 \text{ cm}^{-1}$ region, where the most distinctive spectral features among the different

conformers of the sample are expected to occur, as observed in other related systems previously studied by our group [37,38].

Nevertheless, the $4000\text{--}2600 \text{ cm}^{-1}$ region has also been recorded (Fig. 4). In this region, the broad band assigned to the NH stretching of the H-bonded network appearing at ca. 3300 cm^{-1} in the IR spectra of the sample may indicate the occurrence of hydrogen bond assemblies of oligomeric species of (–)-S-anabasine in the neat liquid. As can be observed, the intensity of this broad band decreases, suggesting the partial disaggregation of the hydrogen bonded network when diluting the sample in CCl_4 .

Fig. 5 collects the experimental VCD and IR spectra recorded for neat liquid (–)-S-anabasine and for its solutions in carbon tetrachloride, in the $1650\text{--}900 \text{ cm}^{-1}$ spectral region. The slight changes in molecular geometries of (–)-S-anabasine conformers expected when increasing the polarity of the surrounding medium (discussed above) and the negligible changes in the conformational composition of the sample made us discard the record of the spectra in DMSO that is also known to strongly interact with solute molecules blurring the interpretation of VCD spectra. For the sake of clarity, all the experimental bands have been marked and labeled according to their experimental wavenumbers. Both VCD and IR spectra recorded for the neat liquid sample and CCl_4 solution look alike (Fig. 5). As shown, there is a good correspondence between

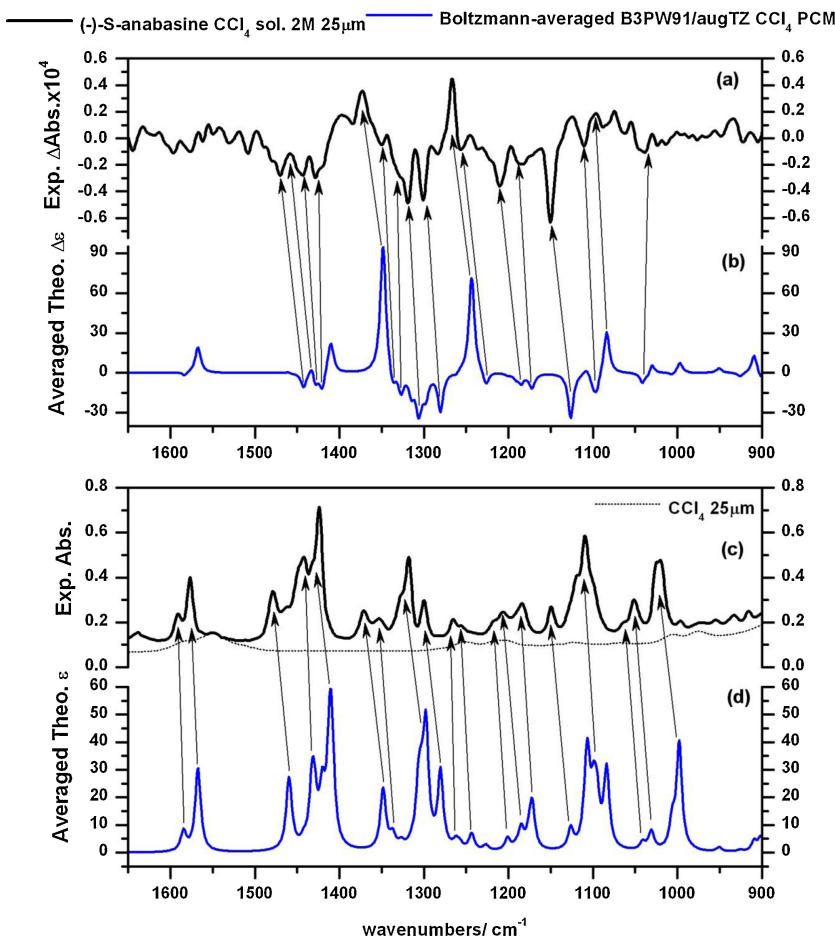


Fig. 7. Experimentally recorded VCD (a) and IR (c) spectra for (*-*)-S-anabasine in carbon tetrachloride solution (black lines) compared with the predicted VCD (b) and IR (d) scaled B3PW91/aug-cc-pVTZ Boltzmann-averaged spectra (blue lines) in the 1650–900 cm^{−1} region for a ca. 2:1 (m01:m02) conformational mixture of the sample in CCl₄. Boltzmann is populations at 298.15K, IEF-PCM $\epsilon = 2.2$, Lorentzian fitted FWHM = 8 cm^{−1}, scale factor = 0.965 taken from the Computational Chemistry Comparison and Benchmark Database, CCCBDB. (For interpretation of the references to color in this figure legend, the reader is referred to the web version of this article.)

the experimental profiles and only slight frequency displacements are observed in certain bands when going from neat liquid to solution. For this reason, we have chosen the neat liquid spectra and gas-phase Boltzmann averaged spectral profile considering the two main conformers as reference for the vibrational assignment (Table 3). We will focus on the results obtained with the B3PW91/aug-cc-pVTZ method for discussion since such functional has been suggested elsewhere [70] as being reliable for computing VCD intensities and in our case performs better than B3LYP mainly in the 1400–1200 cm^{−1} spectral region.

Fig. 6 shows the close theoretical-experimental match reached when comparing the spectra of the pure liquid (*-*)-S-anabasine with the scaled Boltzmann averaged spectra (B3PW91/aug-cc-pVTZ) obtained considering a sample conformational composition of ca. 2:1 (m01:m02). Comparable results are obtained when comparing theoretical and experimental results obtained for the sample in CCl₄ solution (Fig. 7).

The good theoretical reproduction of the experimental spectra allowed assigning the vibrational bands observed in the 1650–900 cm^{−1} region to the following normal modes: $\delta^{ip}CH^{PYR}$, $scCH_2$, δNH^{ip} , $waCH_2$, δC^*H , $twCH_2$, ρCH_2 , νCC^{PYR} , νCCP^{ip} , and $\delta^{oop}CH^{PYR}$ in accordance with their theoretical wavenumbers (Table 3).

As stated above, the calculated VCD and IR profiles for a 2:1 (m01:m02) conformational composition reproduced quite well the experimental spectra of the neat liquid sample and CCl₄ solution. In

Fig. S2 (electronic Supplementary information) it is shown that calculated VCD and IR spectra for isolated conformers m01 and m02 in gas-phase and solution state overlap almost completely in the mid-IR region, being difficult to obtain precise experimental evidences of the occurrence of conformational mixture in the sample. Nonetheless, Fig. 8, which show a comparison between the experimental IR profile in the 1300–1150 cm^{−1} region and two different averaged theoretical spectra taking 2:1 and 1:2 conformational ratios, indeed indicate that the best match is achieved when both conformers contribute to the spectral profile in a 2:1 relative population. The shape and relative intensity of the bands appearing at 1329 cm^{−1} (sh) and 1319 cm^{−1}, which are assigned to the $waCH_2$ and $\delta^{ip}CH^{PYR}$, are consistent with a contribution of ca. 30% of m02. Similarly, the sequence of peaks appearing in the 1200–1150 cm^{−1} region is better justified with a 2:1 Boltzmann averaged theoretical spectrum.

Besides, as shown in Fig. S2, the shape and relative intensity in some spectral regions of the VCD spectra also may confirm the incidence of conformational mixture. For instance, the sequence of $(-) (+) (-) (-)$ peaks appearing in the 1450–1400 cm^{−1} region of the recorded VCD spectrum of the neat liquid sample is matched by the theoretical obtained when a 2:1 combined contribution of m01+m02 conformers is considered.

These features may certainly be an indication of the experimental occurrence of a ca. 2:1 neat liquid and solution-state conformational composition, but unlike what was found for two

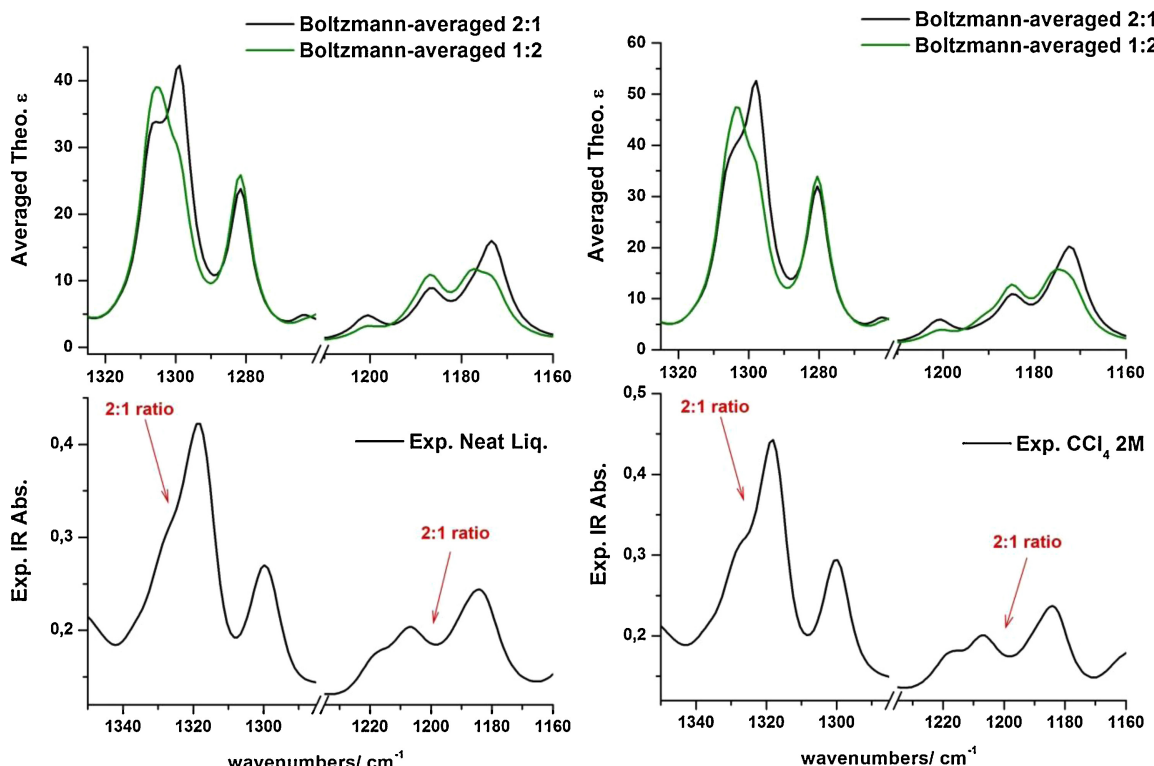


Fig. 8. Comparison of the theoretical averaged IR spectral profile calculated for two different conformational mixtures of (–)-S-anabasine pure (left) and in CCl_4 (right) using B3PW91 functional and the aug-cc-pVTZ basis set (IEF-PCM, Lorentzian function, $\text{FWHM} = 8 \text{ cm}^{-1}$, scale factor = 0.965 taken from the Computational Chemistry Comparison and Benchmark Database, CCCBDB) with the experimental IR spectra recorded for the sample. Effect of the conformational composition on the theoretical-experimental IR resemblance.

chemically related species, namely, (–)-S-nicotine and (–)-S-cotinine [37,38], neither the VCD nor the IR spectra enable us to observe any experimental feature distinctive of each one of the main conformers. The lower populations expected at room temperature for conformers m03 to m08 also prevented the observation of any sign of their presence.

4. Conclusions

Eight different conformations represent minima in the potential energy surface of (–)-S-anabasine. The equatorial disposition of the pyridine ring linked to the C2 in the piperidine ring seems to be the most stability-determinant structural feature in this sort of compounds. Hence, the two main conformers, called m01 and m02, are characterized by the equatorial orientation of the N1–H and C2–Pyr bonds resulting in structures which only differ in the relative rotation of the pyridine ring. These account for *ca.* 97% of the sample composition in gas phase.

Although steric and electrostatic effects are responsible of the higher stability of the two main conformers, hyperconjugative delocalizations, rather than the incidence of intramolecular hydrogen bonding, tip the balance of the conformational equilibrium toward m01, which is the global minimum.

Increasing the polarity of the surrounding medium barely affects the calculated molecular geometries or the conformational energy profile. Nonetheless, it is observed a slight increase in the population of m03 and m04 which is consistent with NBO results that indicate that relative stabilities and abundances of these conformers are controlled mainly by electrostatic effects.

The VCD spectra of (–)-S-anabasine (pure liquid and in CCl_4 solution) have been firstly recorded and assigned. Although no unique and individual spectral features indicating the presence of conformer m02 have been found in the vibrational spectra of

the sample, accurate reproductions of the VCD and IR spectra are obtained from DFT estimations when a 2:1 (m01:m02) relative abundance of the two main conformers is considered, in gas phase and in solution, both in terms of wavenumbers and intensities.

Acknowledgements

Authors thank Andalussian government for funding (FQM-173) and the Centro de Instrumentación Científico Técnico (CICT) of the University of Jaén for instrumental facilities. P. G. R. O. thanks the University of Jaén for a post-doctoral contract supporting this work (Ref. 2014/ CL073 (T2-I)).

Appendix A. Supplementary data

Supplementary data associated with this article can be found, in the online version, at <http://dx.doi.org/10.1016/j.jmgm.2015.05.011>

References

- [1] W.C. Evans Alkaloids, Trease and Evans Pharmacognosy, in: P. Graham (Ed.), Saunders Elsevier, Edinburgh, 2009.
- [2] A.W. Bannon, M.W. Decker, M.W. Holladay, P. Curzon, D. Donnelly-Roberts, P.S. Puttfarcken, R.S. Bitner, A. Diaz, A.H. Dickenson, R.D. Porsolt, M. Williams, S.P. Arneric, Broad-spectrum, non-opioid analgesic activity by selective modulation of neuronal nicotinic acetylcholine receptors, *Science* 279 (1998) 77–81.
- [3] R.M. Eglen, J.C. Hunter, A. Dray, Ions in the fire: recent ion-channel research and approaches to pain therapy, *Trends. Pharm. Sci.* 20 (1999) 337–342.
- [4] S.N. Haydar, C. Ghiron, L. Bettinetti, H. Bothmann, T.A. Cormery, J. Dunlop, S. La Rosa, I. Mico, M. Pollastrini, J. Quinn, R. Roncarati, C. Scali, M. Valacchi, M. Varrone, R. Zanaletti, SAR and biological evaluation of SEN1233/WAY-317538: novel alpha 7 nicotinic acetylcholine receptor agonist, *Bio. Med. Chem.* 17 (2009) 5247–5258.

- [5] H. Yuan, P.A. Petukhov, Computational evidence for the ligand selectivity to the $\alpha 4\beta 2$ and $\alpha 3\beta 4$ nicotinic acetylcholine receptors, *Bioorg. Med. Chem.* 14 (2006) 7936–7942.
- [6] C. Calloe, R. Goodrow, S.P. Olesen, C. Antzelevitch, J.M. Cordeiro, Tissue-specific effects of acetylcholine in the canine heart, *Am. J. Physiol. Heart Circ. Physiol.* 305 (305) (2013) H66–H75.
- [7] A. Kucinski, S. Wersinger, E.K. Stachowiak, M. Radell, R. Hesse, T. Corso, M. Parry, M. Bencherif, K. Jordan, S. Letchworth, M.K. Stachowiak, Unilateral 6-OHDA th-fgrf1 (tk-) mouse model supports the role of FGFs in Parkinson's disease and the effects of nicotine and L-DOPA on spontaneous motor impairments, *Health* 4 (2012) 1178–1190 (and references therein).
- [8] M.N. Tiwari, S. Agarwal, P. Bhatnagar, N.K. Singh, S.K. Tiwari, P. Kumar, L.K.S. Chauhan, D.K. Patel, R.K. Chaturvedi, M.P. Singh, Nicotine-encapsulated poly (lactic-co-glycolic) acid nanoparticles improve neuroprotective efficacy against MPTP-induced parkinsonism, *Free Radic. Biol. Med.* 65 (2013) 704–718 (and references therein).
- [9] (a) M. Stornaiuolo, G.E. De Kloe, P. Rucktooa, A. Fish, R. van Elk, E.S. Edink, D. Bertrand, A.B. Smit, I.J. de Esch, T.K. Sixma, Assembly of a π - π stack of ligands in the binding site of an acetylcholine-binding protein, *Nat. Commun.* 4 (2013) 1875–1886;
 (b) X. Xiu, N.L. Puskar, J.A. Shanata, H.A. Lester, D.A. Dougherty, Nicotine binding to brain receptors requires a strong cation-pi interaction, *Nature* 458 (2009) 534–537.
- [10] V. Tsetlin, F. Hucho, Nicotinic acetylcholine receptors at atomic resolution, *Curr. Opin. Pharmacol.* 9 (2009) 306–310.
- [11] D.L. Beene, G.S. Brandt, W.G. Zhong, N.M. Zacharias, H.A. Lester, D.A. Dougherty, Cation- π interactions in ligand recognition by serotonergic (5-HT3A) and nicotinic acetylcholine receptors: the anomalous binding properties of nicotine, *Biochemistry* 41 (10) (2002) 10262–10269.
- [12] R.J. Radna, D.L. Beveridge, A.L. Bender, Structural chemistry of cholinergic neural transmission systems. II. Quantum theoretical study of the molecular electronic structure of muscarine, nicotine, acetyl-alpha-methylcholine, acetyl-beta-methylcholine, acetyl-a, beta-dimethylcholine, and further studies on acetylcholine, *J. Am. Chem. Soc.* 95 (1973) 3831–3842.
- [13] L.B. Kier, A molecular orbital calculation of the preferred conformation of nicotine, *J. Mol. Pharmacol.* 4 (1968) 70–76.
- [14] B. Pullman, P. Courrière, J.L. Coubeils, Quantum mechanical study of the conformational and electronic properties of acetylcholine and its agonists muscarine and nicotine, *J. Mol. Pharmacol.* 7 (1971) 397–405.
- [15] M. Berthelot, M. Decouzon, J.F. Gal, C. Laurence, J.V. Le Questel, P.C. Maria, J. Tortajada, Gas-phase basicity and site of protonation of polyfunctional molecules of biological interest: FT-ICR experiments and AM1 calculations on nicotines nicotinic acid derivatives, and related compounds, *J. Org. Chem.* 56 (1991) 4490–4494.
- [16] D.E. Elmore, D.A. Dougherty, A computational study of nicotine conformations in the gas phase and in water, *J. Org. Chem.* 65 (2000) 742–747.
- [17] J. Graton, M. Berthelot, J.F. Gal, S. Girard, C. Laurence, J. Lebreton, J.Y. Le Questel, P.C. Maria, P. Naus, Site of protonation of nicotine and nornicotine in the gas phase: pyridine or pyrrolidine nitrogen? *J. Am. Chem. Soc.* 124 (2002) 10552–10562.
- [18] T. Takeshima, R. Fukumoto, T. Egawa, S. Konata, Molecular structure of nicotine as studied by gas electron diffraction combined with theoretical calculations, *J. Phys. Chem. A* 106 (2002) 8734–8740.
- [19] M. Mora, M.E. Castro, A. Niño, F.J. Meléndez, C. Muñoz-Caro, Analysis of B3LYP and MP2 conformational population distributions in trans-nicotine acetylcholine, and ABT-594, *Int. J. Quant. Chem.* 103 (2005) 25–33.
- [20] T. Yoshida, W.A. Farone, S.S. Xantheas, Isomers and conformational barriers of gas-phase nicotine, nornicotine, and their protonated forms, *J. Phys. Chem. B* (2014). <http://dx.doi.org/10.1021/jp501646p>
- [21] C. Eddy, C. Roland, A. Eisner, Infrared spectra of nicotine and some of its derivatives, *Anal. Chem.* 26 (1954) 1428–1431.
- [22] E. Wada, K. Yamasaki, M. Lida, K. Saito, Y. Nakayama, Tobacco alkaloids. Infrared absorption spectra of the tobacco alkaloids and some related compounds, *Nippon Senbai Kosha Chuo Kenkyusho* 97 (1957) 27–39.
- [23] M. Dezelic, N. Branko, Determination of structure of some salts of nicotine, pyridine and N-methylpyrrolidine on the basis of their infra-red spectra, *Spectrochim. Acta A* 23 (1967) 1149–1153.
- [24] M. Seydou, G. Gregoire, J. Liquier, J. Lemaire, J.P. Schermann, C. Desfrançois, Experimental observation of the transition between gas-phase and aqueous solution structures for acetylcholine nicotine, and muscarine ions, *J. Am. Chem. Soc.* 130 (2008) 4187–4195.
- [25] M. Baranska, J. Cz Dobrowski, A. Kaczor, K. Chruszcz-Lipska, K. Gorz, A. Rygula, Tobacco alkaloids analyzed by Raman spectroscopy and DFT calculations, *J. Raman Spectrosc.* 43 (2012) 1065–1073.
- [26] J.U. Grabow, S. Mata, J.L. Alonso, I. Pena, S. Blanco, J.C. Lopez, C. Cabezas, Rapid probe of the nicotine spectra by high-resolution rotational spectroscopy, *Phys. Chem. Chem. Phys.* 13 (2011) 21063–21069.
- [27] P.S. Hammond, Y. Wu, R. Harris, T.J. Minehardt, R. Car, J.D. Schmitt, Protonation-induced stereoisomerism in nicotine: conformational studies using classical (AMBER) and ab initio (Car-Parrinello) molecular dynamics, *J. Comput. Aided Mol. Des.* 19 (19) (2005) 1–15.
- [28] M. Koné, B. Illien, C. Laurence, J.-F. Gal, P.-C. María, Are nicotinoids protonated on the pyridine or the amino nitrogen in the gas phase? *J. Phys. Org. Chem.* 19 (2006) 104–114.
- [29] J.D. Schmitt, C.G.V. Sharples, W.S. Caldwell, Molecular recognition in nicotinic acetylcholine receptors: The importance of π -cation interactions, *J. Med. Chem.* 42 (1999) 3066–3074.
- [30] S.B. Soloway, Naturally occurring insecticides, *Env. Health Perspect.* 14 (1976) 109–117.
- [31] T.K. Yunusov, A.P. Matveeva, V.B. Leont'ev, F.G. Kamaev, A. Kh. Aslanov, A.S. Saykov, Comparative study of the IR spectra of alkaloids containing piperidine and quinolizidine rings in the 2500–2830 cm⁻¹ range, *Khimiya Prirodnnykh Soedinenii* 2 (1972) 200–207.
- [32] O.I. Granitova, G.S. Dordzhin, Infrared spectrum of anabasine, *Nauchn. Tr. Tashkentsk. Gos. Univ.* 257 (1964) 55–63.
- [33] E. Wada, K. Yamasaki, M. Lida, K. Saito, Y. Nakayama, Tobacco alkaloids. Infrared absorption spectra of the tobacco alkaloids and some related compounds, *Kenkyu Hokoku – Nippon Senbai Kosha Chuo Kenkyusho* 97 (1957) 27–39.
- [34] W. Wojciechowska-Nowak, U. Rychlewska, B. Warzajtis, Spectroscopy and crystal structure of anabasine salts, *J. Mol. Struct.* 840 (2007) 44–52.
- [35] A. Lesarri, E.J. Cocinero, L. Evangelisti, R.D. Suehring, W.R. Caminati, J.-U. Grabow, The conformational landscape of nicotinoids: solving the conformational disparity of anabasine, *Chem. Eur. J.* 16 (10) (2010) 214–219.
- [36] M. Baranska, J. Cz Dobrowski, A. Kaczor, K. Chruszcz-Lipska, K. Gorz, A. Rygula, Tobacco alkaloids analyzed by Raman spectroscopy and DFT calculations, *J. Raman Spectrosc.* 43 (2012) 1065–1073.
- [37] P.G. Rodríguez Ortega, M. Montejano, J.J. López González, Vibrational Circular Dichroism and theoretical study of the conformational equilibrium in ($-$)-S-nicotine, *ChemPhysChem* 16 (2015) 342–352.
- [38] P.G. Rodríguez Ortega, M. Montejano, F. Márquez, J.J. López González, DFT-aided vibrational circular dichroism spectroscopy study of the conformational preference, rotational isomerism and solution-state conformer distribution of ($-$)-S-cotinine, *ChemPhysChem* 16 (2015) 1416–1427.
- [39] T.A. Halgren, Merck molecular force field. I. Basis form scope, parameterization, and performance of MMFF94, *J. Comput. Chem.* 17 (1995) 490–519.
- [40] T.A. Halgren, Merck molecular force field. II. MMFF94 van der Waals and electrostatic parameters for intermolecular interactions, *J. Comput. Chem.* 17 (1995) 520–552.
- [41] T.A. Halgren, Merck molecular force field. III. Molecular geometries and vibrational frequencies for MMFF94, *J. Comput. Chem.* 17 (1995) 553–586.
- [42] T.A. Halgren, R.B. Nachbar, Merck molecular force field. IV. Conformational energies and geometries for MMFF94, *J. Comput. Chem.* 17 (1995) 587–615.
- [43] T.A. Halgren, Merck molecular force field. V. Extension of MMFF94 using experimental data additional computational data, and empirical rules, *J. Comput. Chem.* 17 (1995) 616–641.
- [44] M. Clark, R.D. Cramer, N.V. Opdenbosch, Validation of the general purpose Tripos 5.2 force field, *J. Comput. Chem.* 10 (1989) 982–1012.
- [45] Y. Shao, L.F. Molnar, Y. Jung, J. Kussmann, C. Ochsenfeld, S.T. Brown, A.T.B. Gilbert, L.V. Slipchenko, S.V. Levchenko, D.P. O'Neill, R.A. DiStasio Jr., R.C. Lochan, T. Wang, G.J.O. Beran, N.A. Besley, J.M. Herbert, C.Y. Lin, T. Van Voorhis, S.H. Chien, A. Sodt, R.P. Steele, V.A. Rassolov, P.E. Maslen, P.P. Korambath, R.D. Adamson, B. Austin, J. Baker, E.F.C. Byrd, H. Dachs, R.J. Doerksen, A. Dreuw, B.D. Dunietz, A.D. Dutoi, T.R. Furlani, S.R. Gwaltney, A. Heyden, S. Hirata, C.-P. Hsu, G. Kedziora, R.Z. Khalil, P. Klunzinger, A.M. Lee, M.S. Lee, W.Z. Liang, I. Lotan, N. Nair, B. Peters, E.I. Proynov, P.A. Pieniazek, Y.M. Rhee, J. Ritchie, E. Rosta, C.D. Sherrill, A.C. Simmonett, J.E. Subotnik, H.L. Woodcock III, W. Zhang, A.T. Bell, A.K. Chakraborty, D.M. Chipman, F.J. Keil, A. Warshel, W.J. Hehre, H.F. Schaefer, J. Kong, A.I. Krylov, P.M.W. Gill, M. Head-Gordon, *Phys. Chem. Chem. Phys.* 8 (2006) 3172, Spartan'08 Wavefunction, Inc., Irvine, CA.
- [46] M.J. Frisch, G.W. Trucks, H.B. Schlegel, G.E. Scuseria, M.A. Robb, J.R. Cheeseman, G. Scalmani, V. Barone, B. Mennucci, G.A. Petersson, H. Nakatsuji, M. Caricato, X. Li, W.H. Pritchard, A.F. Izmaylov, J. Bloino, G. Zheng, J.L. Sonnenberg, M. Hada, M. Ehara, K. Toyota, R. Fukuda, J. Hasegawa, M. Ishida, T. Nakajima, Y. Honda, O. Kitao, H. Nakai, T. Vreven, J.A. Montgomery Jr., J.E. Peralta, F. Ogliaro, M. Bearpark, J.J. Heyd, E. Brothers, K.N. Kudin, V.N. Staroverov, T. Keith, R. Kobayashi, J. Normand, K. Raghavachari, A. Rendell, J.C. Burant, S.S. Iyengar, J. Tomasi, M. Cossi, N. Rega, J.M. Millam, M. Klene, J.E. Knox, J.B. Cross, V. Bakken, C. Adamo, J. Jaramillo, R. Gomperts, R.E. Stratmann, O. Yazyev, A.J. Austin, R. Cammi, C. Pomelli, J.W. Ochterski, R.L. Martin, K. Morokuma, V.G. Zakrzewski, G.A. Voth, P. Salvador, J.J. Dannenberg, S. Dapprich, A.D. Daniels, O. Farkas, J.B. Foresman, J.V. Ortiz, J. Cioslowski, D.J. Fox, Gaussian 09 (Revision D.01), Gaussian, Inc., Wallingford CT, 2013.
- [47] A.D. Becke, Density-functional thermochemistry. III. The role of exact exchange, *J. Chem. Phys.* 98 (1993) 5648–5652.
- [48] C. Lee, W. Yang, R.G. Parr, Development of the Colle-Salvetti correlation-energy formula into a functional of the electron density, *Phys. Rev. B* 37 (1998) 785–789.
- [49] J.P. Perdew, J.A. Chevary, S.H. Vosko, K.A. Jackson, M.R. Pederson, D.J. Singh, C. Fiolhais, Atoms molecules, solids, and surfaces: Applications of the generalized gradient approximation for exchange and correlation, *Phys. Rev. B* 46 (1992) 6671–6687.
- [50] P. Perdew, K. Burke, Y. Wang, Generalized gradient approximation for the exchange-correlation hole of a many-electron system, *Phys. Rev. B* 54 (1996) 16533.
- [51] J.F. Dobson, G. Vignale, M.P. Das, Electronic Density Functional Theory: Recent Progress and New Directions, Plenum, 1998.

- [52] D. McLean, G.S. Chandler, Contracted Gaussian basis sets for molecular calculations. I. Second row atoms, $Z=11-18$, *J. Chem. Phys.* 72 (1980) 5639–5648.
- [53] R.A. Kendall, T.H. Dunning Jr., R.J. Harrison, Electron affinities of the first-row atoms revisited. Systematic basis sets and wave functions, *J. Chem. Phys.* 96 (1992) 6796–6806.
- [54] J.S. Binkley, J.A. Pople, Møller-Plesset theory for atomic ground state energies, *Int. J. Quantum Chem.* 9 (1975) 229–236.
- [55] G.A. Petersson, A. Bennett, T.G. Tensfeldt, M.A. Al-Laham, W.A. Shirley, J. Mantzaris, A complete basis set model chemistry. I. The total energies of closed-shell atoms and hydrides of the first-row elements, *J. Chem. Phys.* 89 (1988) 2193–2218.
- [56] G.A. Petersson, M.A. Al-Laham, A complete basis set model chemistry. II. Open-shell systems and the total energies of the first-row atoms, *J. Chem. Phys.* 94 (1991) 6081–6090.
- [57] E. Reed, L.A. Curtiss, F. Weinhold, Intermolecular interactions from a natural bond orbital, donor–acceptor viewpoint, *Chem. Rev.* 88 (1988) 899–926.
- [58] E.D. Glendening, J.K. Badenhoop, A.E. Reed, J.E. Carpenter, J.A. Bohmann, C.M. Morales, C.R. Landis, F. Weinhold, NBO 6.0: Natural Bond Orbital Analysis Program, Theoretical Chemistry Institute, University of Wisconsin, Madison, WI, USA, 2013.
- [59] S. Miertsch, E. Scrocco, J. Tomasi, Electrostatic interaction of a solute with a continuum. A direct utilization of AB initio molecular potentials for the prevision of solvent effects, *Chem. Phys.* 55 (1981) 117–129.
- [60] J. Tomasi, B. Mennucci, R. Cammi, Quantum mechanical continuum solvation models, *Chem. Rev.* 105 (2005) 2999–3094.
- [61] B. Mennucci, E. Cancès, J. Tomasi, Evaluation of solvent effects in isotropic and anisotropic dielectrics and in ionic solutions with a unified integral equation method: theoretical bases computational implementation, and numerical applications, *J. Phys. Chem. B* 101 (1997) 10506–10517.
- [62] E. Cancès, B. Mennucci, J. Tomasi, A new integral equation formalism for the polarizable continuum model: Theoretical background and applications to isotropic and anisotropic dielectrics, *J. Chem. Phys.* 107 (1997) 3032–3041.
- [63] E. Cancès, B. Mennucci, New applications of integral equations methods for solvation continuum models: ionic solutions and liquid crystals, *J. Math. Chem.* 23 (1998) 309–326.
- [64] L.A. Nafie, *Vibrational Optical Activity: Principles and Applications* (Chapter 8: Measurement of Vibrational Optical Activity), Wiley, John Wiley & Sons Ltd., 2011.
- [65] P.J. Stephens, F.J. Devlin, J.R. Cheeseman, *VCD Spectroscopy for Organic Chemists* (Chapter 2: The experimental measurement of Vibrational Absorption and Vibrational Circular Dichroism Spectra), CRC Press, Taylor & Francis Group, Boca Raton, 2012.
- [66] L. Carballera, I. Pérez-Juste, Ab initio study of the axial/equatorial equilibrium in *N*- and *O*-containing rings in gas phase and aqueous solution: 1-oxa-3-aza-, 1-oxa-3 5-diaza-, 1, 3-dioxa-5-azacyclohexanes and *N*-methyl derivatives, *J. Org. Chem.* 62 (1997) 6144–6151.
- [67] R. Taylor, O. Kennard, Crystalllographic evidence for the existence of CH-O, CH-N and CH-Cl hydrogen bonds, *J. Am. Chem. Soc.* 104 (1982) 5063–5070.
- [68] J. Graton, M. Berthelot, J.-F. Gal, S. Girard, C. Laurence, J. Lebreton, J.-Y. Le Questel, P.-C. Maria, P. Naus, Site of protonation of nicotine and nornicotine in the gas phase: pyridine or pyrrolidine nitrogen? *J. Am. Chem. Soc.* 124 (2002) 10552–10562.
- [69] J.S. Brodbelt, J. Isbell, J.M. Goodman, H.V. Secor, J.I. Seeman, Gas-Phase versus solution chemistry: on the reversal of regiochemistry of methylation of sp^2 and sp^3 nitrogens, *Tet. Lett.* 42 (2001) 6949–6952.
- [70] P.J. Stephens, F.J. Devlin, J.R. Cheeseman, *VCD Spectroscopy for Organic Chemists* (Chapter 4: ab initio Methods and Chapter 5: Analyses of the IR and VCD Spectra of Conformationally Rigid Molecules), CRC Press, Taylor & Francis Group, Boca Raton, 2012.